Kovove Mater. 60 2022 351–362
DOI: 10.31577/km.2022.6.351

Waste metals based metal-matrix ceramic-reinforced composites for friction applications

Mária Podobová, Viktor Puchý, Ladislav Falat*, Róbert Džunda, Michal Besterci

Institute of Materials Research, Slovak Academy of Sciences, Watsonova 47, 04001 Košice, Slovak Republic

Received 14 September 2022, received in revised form 21 October 2022, accepted 24 October 2022

Abstract

The possibility of reusing waste metals as alternative raw materials for producing materials for friction applications was investigated. The Ti-matrix composites containing 40 wt.% of waste Ti with fixed powder additions of 25 wt.% Fe, 10 wt.% ZrO_2, 5 wt.% SiC, 5 wt.% graphene nanoplatelets (GNPs), and 15 wt.% of alternative additions of waste metallic materials, namely MgAl, CuZn, Al, were prepared by mechanical milling and mixing of powders and subsequent compactization using spark plasma sintering (SPS) technique in vacuum at process parameters 1000 °C and 50 MPa for 10 min. As confirmed by microstructural and tribological analyses, all studied composites exhibited satisfactory average hardness values (220–350 HV 5) and coefficient of friction (0.5–0.7). Obtained results on wear resistance indicated that among all the currently studied composites, the developed metal-ceramic composite 40Ti-25Fe-15MgAl-10ZrO_2-5SiC-5GNPs has the most promising potential to be applied for intended friction applications.

K e y w o r d s: metal matrix composites, metal waste reuse, SPS, friction, wear, graphene

1. Introduction

Brakes are mechanical devices used to slow down, stop moving, or prevent motion [1, 2]. Materials for friction applications represent two surfaces pressed together. During this process, friction occurs. This movement converts kinetic energy into heat, electrical energy, and potential energy, which can be stored for later use. Also, the kinetic energy from braking can be transformed into the energy of a rotating flywheel. The brake performance of a vehicle is determined by the tribological properties between the brake system and braking pad [3–5]. The exact chemical composition of commercial friction materials is not commonly available in the freely available literature. Friction composites can be manufactured from different types of materials. They are designed as so-called multi-ingredient composite materials with the addition of reinforcements [6–8]. These play an important role in achieving high friction coefficients and good wear resistance during braking. Friction composites can be characterized by the main component as semi-metallic, non-asbestos (NAO), low-metallic NAO, and ceramic. NAO, also called organic, is made from organic fibers like carbon, rubber, glass or Kevlar with high-temperature resistance. Low-metallic NAO is made from organic matter with the addition of 10–30 wt.% of copper or steel wool to increase thermal conductivity. Semi-metallic brake pads are from 30–65 wt.% metallic. It is a mixture of shredded copper, iron dust and steel wool with friction modifiers. Unfortunately, these are louder, with low efficiency at low temperatures. Ceramic brake pads are quiet and clean, with excellent braking effects. They tend to produce less dust and other particles as they wear down in time. They can be used in a wider temperature range and driving conditions. Although they have fine copper fibers to help increase friction and heat conductivity, there are some limitations. They tend to be expensive. Moreover, ceramics and copper cannot absorb as much heat as other materials. This often results in more intensive wear of braking components. Ceramic brake pads are unsuitable for extreme driving conditions, e.g., freezing climates. Metallic brake pads consist of 30–70 % metals like copper, iron, steel or other composite alloys. These are combined with graphite lubricant and other

*Corresponding author: e-mail address: lfalat@saske.sk

fillers. The compounds offer their advantages for different situations. Metallic brake pads offer improved braking performance in a much wider range of temperatures and conditions. Metals are good heat conductors and do not compress like organic brakes. Therefore, there is a need for less pressure to affect stopping ability. But there are also some disadvantages. They tend to be louder than ceramic brake pads and also produce more brake dust [9]. The main friction composite parameters we must focus on are working temperature, friction coefficient, wear resistance, corrosion resistance, etc., during friction [10, 11]. Nowadays, increased interest is focused on criteria guaranteeing low-cost and environmentally friendly production. Due to depleting natural raw materials resources and environmental protection requirements, manufacturers and researchers are permanently looking for new materials and their combinations to produce composites with desirable functional properties and minimal effects on the environment and human health [12]. One of the possible approaches for friction composite design is focused on using waste materials from other manufacturing processes, e.g., machining operations, as additive ingredients [13]. Among other things, safety requirements, the long life of the brake parts, and high comfort (dynamic and acoustic aspects) are not lacking interest [14–16]. Possible metallic waste materials for use in such applications can be, for instance, titanium, aluminum, copper, stainless steel, or any commercial non-ferrous metallic materials, e.g., MgAl, CuZn, etc., in the form of chips, fibers or powders. Titanium can be used due to its excellent strength, high elastic modulus, wear resistance, and chemical and thermal resistance. Aluminum replaces iron and other metals due to its low weight, high strength, and corrosion resistance. Copper and its alloys have various uses that reflect their versatile physical, mechanical, and chemical properties. Copper has high thermal conductivity and good corrosion resistance. Stainless steel in the form of sawdust is highly corrosion-resistant. CuZn alloys have good resistance to corrosion in the atmosphere, sea water, and overheated steam. The cost of copper-based alloys is generally higher than that of steels but lower than that of nickel-based alloys. MgAl alloys are light and possess good mechanical strength and thermal conductivity. All these materials are promising for a wide range of use, e.g., friction materials, structural materials, wear-resistant parts, etc. Previous experiments on adding Ti machining waste in the form of fibers or chips into Cu-Fe based metal matrix composite, with the addition of ZrO_2, SiC, and graphite, resulted in a beneficial effect on friction coefficient (COF). But it is necessary to focus on ensuring higher microstructure homogeneity of the prepared composites, e.g., by using high-energy ball milling [17]. The brake performance is affected not only by individual components but also by manufacturing process and parameters, which is considered the second source of heterogeneity [18].

Table 1. Experimental composites composition (wt.%)

Composite components	A1*	A2**	A3***
Ti	40	40	40
Fe	25	25	25
MgAl	15	–	–
CuZn	–	15	–
Al	–	–	15
ZrO_2	10	10	10
SiC	5	5	5
GNPs	5	5	5

*A1 – 40Ti-25Fe-15MgAl-10ZrO_2-5SiC-5GNPs
**A2 – 40Ti-25Fe-15CuZn-10ZrO_2-5SiC-5GNPs
***A3 – 40Ti-25Fe-15Al-10ZrO_2-5SiC-5GNPs

In the present work, experimental SPS-fabricated Ti-Fe metal matrix composites with the addition of Al, CuZn, MgAl, graphene nanoplatelets (GNPs), ZrO_2, and SiC were studied. The main aim of this work was to examine the use of selected alternative metallic waste materials incorporated into the Ti-Fe metal matrix to determine their use in friction composites concerning the required tribological properties and to highlight the possibilities for recycling these waste materials in materials for friction applications.

2. Experimental materials and methods

Our experimental materials represent the combination of metal-matrix (Ti, Fe) with the addition of ceramics (ZrO_2, SiC) and waste metallic materials (Al, CuZn, MgAl). The addition of 5 wt.% of GNPs was used to enhance the friction behavior. The exact composition of our three experimental composites in wt.% can be seen in Table 1. Three different mixtures of Ti-Fe-based metal matrix composite materials were produced by spark plasma sintering (SPS). The experimental composites (Table 1) were designed with regard to their required properties, e.g., high thermal conductivity and reduced fading behavior.

The characteristics of raw materials used to prepare investigated composites are given in Table 2.

Figure 1 shows the morphologies of the four input waste materials before adding them into the UFO disc mill. The waste Ti exhibits variously sized and shaped chips morphology, as shown in Fig. 1a. The MgAl exhibits irregular morphology, variously sized chips and shavings (see Fig. 1b). Figure 1c shows the morphology of CuZn powder with the average particle size of 35 μm. Figure 1d shows the spherical Al powder with a particle size of around 50 μm.

During the braking, friction-related heat genera-

Table 2. Characterization of raw materials used for the preparation of investigated composites

Raw material	Size and form	Purity	Supplier
Ti	Variously sized and shaped chips	98 % Ti, impurities: Fe, Al, V, Ni, and oil from machining	Pkchemie-kovyachemie.cz
Fe	Powder with 45 μm grain size	99.9 % Fe, grade: ASC 100.29	Höganäs AB Sweden
MgAl	Variously sized chips and shavings	89.5–91 % Mg, 7.5– 9 % Al, about 1 % of impurities: Zn, Mn, Cu	Pkchemie-kovyachemie.cz
CuZn	Powder with 35 μm average grain size	Cu > 70 %, Zn stabilized > 30 %	Pkchemie-kovyachemie.cz
Al	Powder with 50 μm average grain size	min. 99.4 % Al, max. 0.11 % Si, max. 0.07 % Cu	Pkchemie-kovyachemie.cz
ZrO_2	Powder with 5 μm grain size	99 % ZrO_2	Sigma Aldrich
SiC	β-SiC powder with 0.5 μm grain size	99.9 % SiC	HC Starck
GNPs	Synthetic with 20 μm grain size		Sigma Aldrich

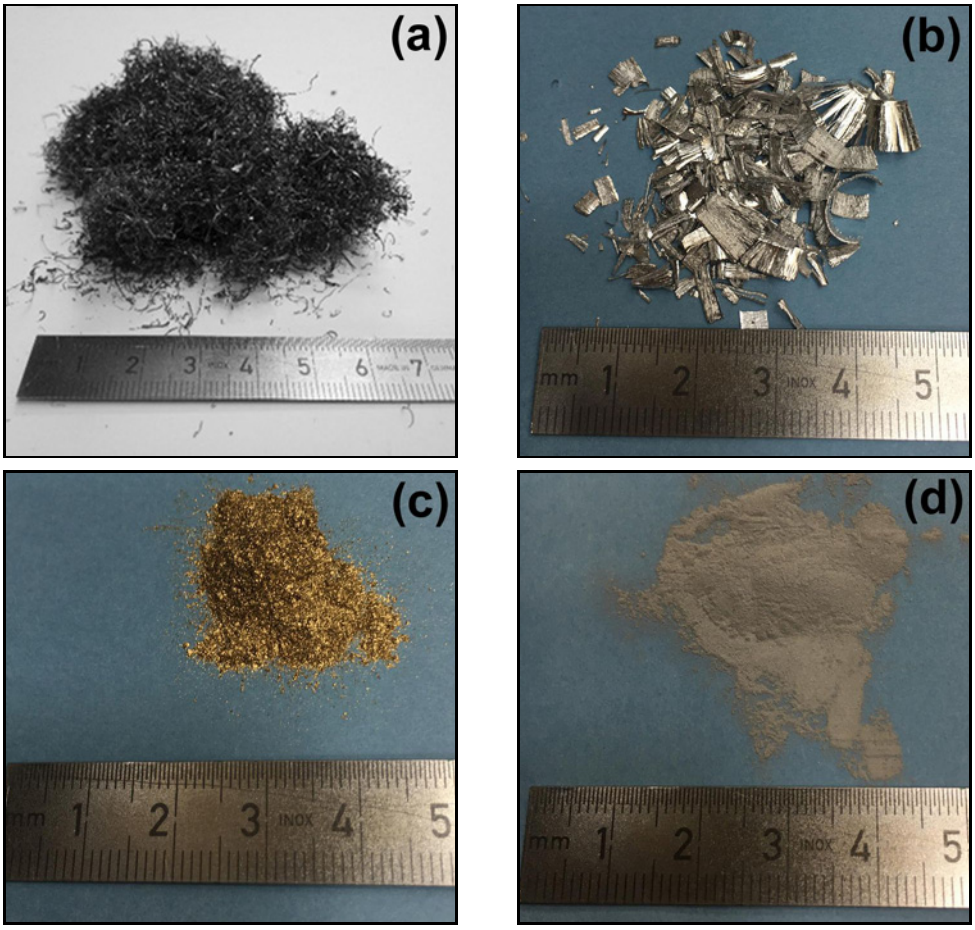

Fig. 1. Morphologies of input waste materials used for SPS fabrication of investigated composites: (a) Ti-chips, (b) MgAl alloy chips and shavings, (c) CuZn powder, and (d) Al powder.

tion occurs. Copper addition within the experimental composites is responsible for increasing the thermal conductivity. CuZn, in addition to it, has very good corrosion resistance. Thus, the more efficient cooling of the brake components, as well as considerable improvement of their braking efficiency, can be possibly obtained. Titanium has been added due to its very good wear and chemical and thermal resistance. Adding Al is helpful where high strength at a low weight is required. MgAl alloy is lighter and stronger and provides better heat conduction. The addition of ceramic powders, such as ZrO_2 and SiC, aims to improve hardness and friction behavior. The optimal coefficient of friction (COF) of brake materials has to be 0.3–0.7 in dry friction systems. The ceramic abrasives ZrO_2 and SiC improve the cold friction behavior.

On the other hand, the graphene nanoplatelets (GNPs) act like a lubricant lowering the friction level via the building-up of friction films. It also improves corrosion resistance and is like an anti-noise agent on the friction surface. For each experimental composite composition, the powder mixture was added into the so-called UFO disc mill (WAB AG, Switzerland) for 2×5 min. Before mixing with other ingredients, the Ti-chips were ultrasonically cleaned in perchloroethylene. The mixed composite powder was loaded into a graphite mold with an inside diameter of 20 mm. The SPS machine (HP D 10SD, FCT Systeme, Germany) was used to sinter prepared mixtures in a vacuum (5 Pa). A pulsed direct electric current was applied with a pulse duration of 15 ms and a pause time of 3 ms throughout all sintering experiments. The temperature was measured using a top pyrometer focused inside a hole in the punch at a distance of 4 mm from the sample. The mold/punch assembly was wrapped in a graphite insulating foil and placed in the SPS. The powder was then heated in low vacuum condition (10 Pa). The sintering temperature was 1000 ℃, the heating rate 100 ℃ min^{-1}, the dwelling time 10 min, and the applied pressure 50 MPa. The composite samples were sintered as discs with a diameter of 20 mm and thickness of 4 mm. All the ceramic discs were ground, followed by polishing with a series of SiC abrasive papers down to 3 μm. After these processes, they were polished with diamond paste to smooth the surface. The apparent density was measured as a ratio between the apparent volume and dry mass of prepared samples. Microhardness was determined according to the Vickers hardness method at 500 g loading for 10 s per measurement. The microstructure of the sintered composites was analyzed using a light optical microscope Olympus GX 71 and scanning electron microscope (SEM) Tescan Vega-3 LMU, equipped with an energy dispersive X-ray spectrometer (EDXS) Bruker XFlash Detector 410-M for area-elemental chemical composition analysis. Also, scanning electron microscopy (SEM, JEOL JSM-7000F, Netherlands) was equipped with an energy dispersive spectrometer (EDS) system for microstructure examination and spot elemental chemical composition analysis. The X-ray diffraction (XRD) phase analyses of investigated composites were performed using a Philips X'Pert Pro diffractometer (Panalytical B.V., Almelo, The Netherlands) using Cu-Kα radiation. The friction and wear behavior of the composites were studied by using a tribometer HTT by CSM Instruments in the air at room temperature, employing a common "ball-on-disc" technique. The tribological partner for each tested material was a polished ball with a 6 mm diameter, made of conventional bearing steel, corresponding to the counter-part material in real brake systems. The applied load was 3 N, the sliding speed ranged from 100 to 300 mm s^{-1}, and the sliding distance was 500 m. The wear resistance for individual experimental composites at used sliding speeds was determined by measuring the average weight loss using analytical balance KERN ABJ 120-4M with a nominal accuracy of ± 0.0001 g. The morphology of worn surfaces and wear mechanisms was analyzed using a confocal 3D Optical Profiler (PLu neox, SENSOFAR). The chemical composition of composite samples was prepared by SPS and the original recycled powder was determined by EDXS analysis.

3. Results and discussion

3.1. Sintering behavior, microstructure, morphology, and components distribution

Figure 2 shows the SEM-EDXS mapping of three milled powder mixtures of friction composites. It indicates that all powders were dispersed uniformly in the titanium matrix for all the mixtures.

As shown by the EDXS results for samples A1, A2, and A3, the large red and purple particles are titanium. The dispersed green particles are graphene nanoplatelets. The good distribution of GNPs in the matrix was found in all composite powder materials. This potentially can create an electrically conductive grid that can enhance the sintering process. The sintering curves (shrinkage vs time) of the spark plasma sintered composites A1–A3 according to the one-step loading cycle and sintering temperature and force vs time are presented in Figs. 3 and 4, respectively. Dense materials were obtained from the samples sintered according to the one-step loading cycle. The densification curve of the samples shows a densification behavior. The densification process starts approx. at 450 ℃, reached already at 750 ℃ in the case of A3, which is about 250 ℃ under setting sintering temperature, and in the case of samples A1 and A2 after reaching setting sintering temperature at 1000 ℃.

The microstructures of individual sintered compos-

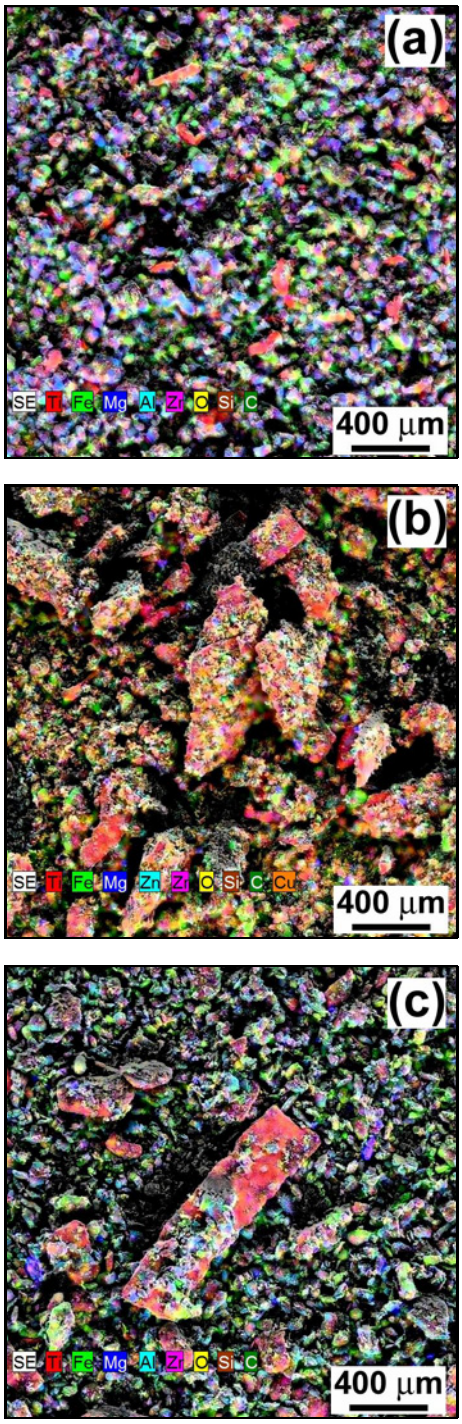

Fig. 2. EDXS mapping of three milled composite powder mixtures after milling in the UFO disc mill: (a) composite A1, (b) composite A2, and (c) composite A3.

ites produced by SPS are shown in Fig. 5.

Light-optical microstructural analyses showed that dense microstructures with very low porosity were found in all sintered materials. Figure 5 indicates that the porosity of produced SPS composites is less than 1 %. The measured values of hardness and apparent

Table 3. Hardness and apparent density of studied composites

Composite	Hardness HV 5	Apparent density (g cm^{-3})
A1	310.8 ± 114.3	4.568
A2	220.8 ± 99.9	4.832
A3	349.4 ± 107.2	4.897

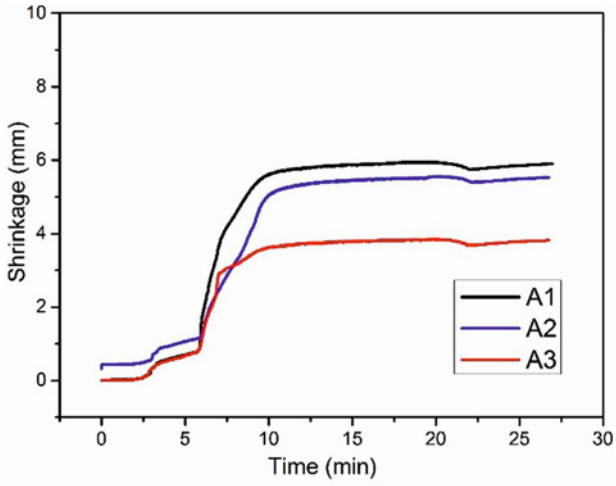

Fig. 3. Sintering curves showing shrinkage vs time for studied composites A1, A2, and A3.

density of studied composites are shown in Table 3.

It can be stated that the selected sintering parameters (1000 ℃, 50 MPa, 10 min) of the used SPS process for the production of studied composites were capable of ensuring the highest possible compaction. It is seen that the microhardness is higher for the composites A1 and A3 and lower for the composite A2 (Table 3). Moreover, for the prepared composites, it was observed that for the same sintering temperature, the microhardness of the sample containing Al is slightly higher than for the samples containing MgAl and CuZn (see Table 3). However, the measured hardness values exhibit large scatter bands in all cases because the grain size of titanium particles is much larger than the grain size of the other fine powders. Thus the large-grain titanium vastly influences the microhardness value scattering of Ti-matrix composites. It is clear that for all composites, the apparent density and microhardness change with the individual additive. Compared to the sample with aluminum, the effect of the use of GNPs on the microhardness of the prepared composites is significantly greater for Al additive than for MgAl and CuZn. This is probably related to the fact that in the case of graphene additive, the application of pressure has a significantly greater effect on the compaction of composite with Al than in the case of composites with CuZn and MgAl addi-

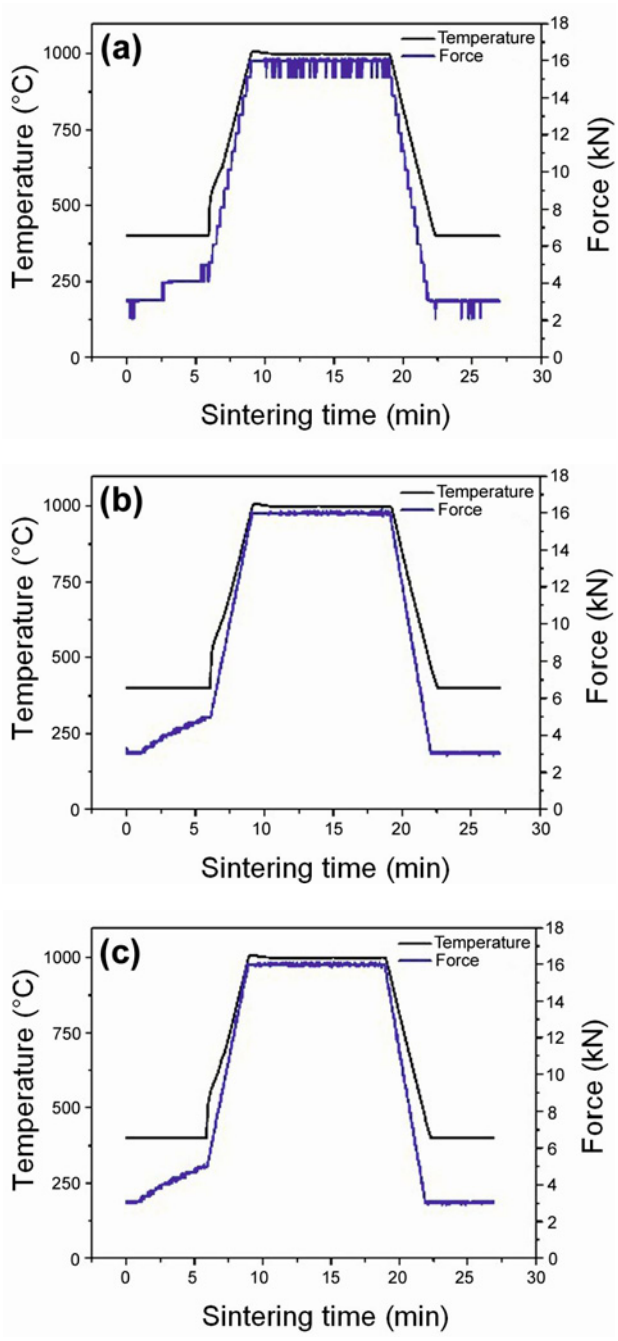

Fig. 4. Sintering curves showing sintering temperature and force vs time for individual compositions: (a) composite A1, (b) composite A2, and (c) composite A3.

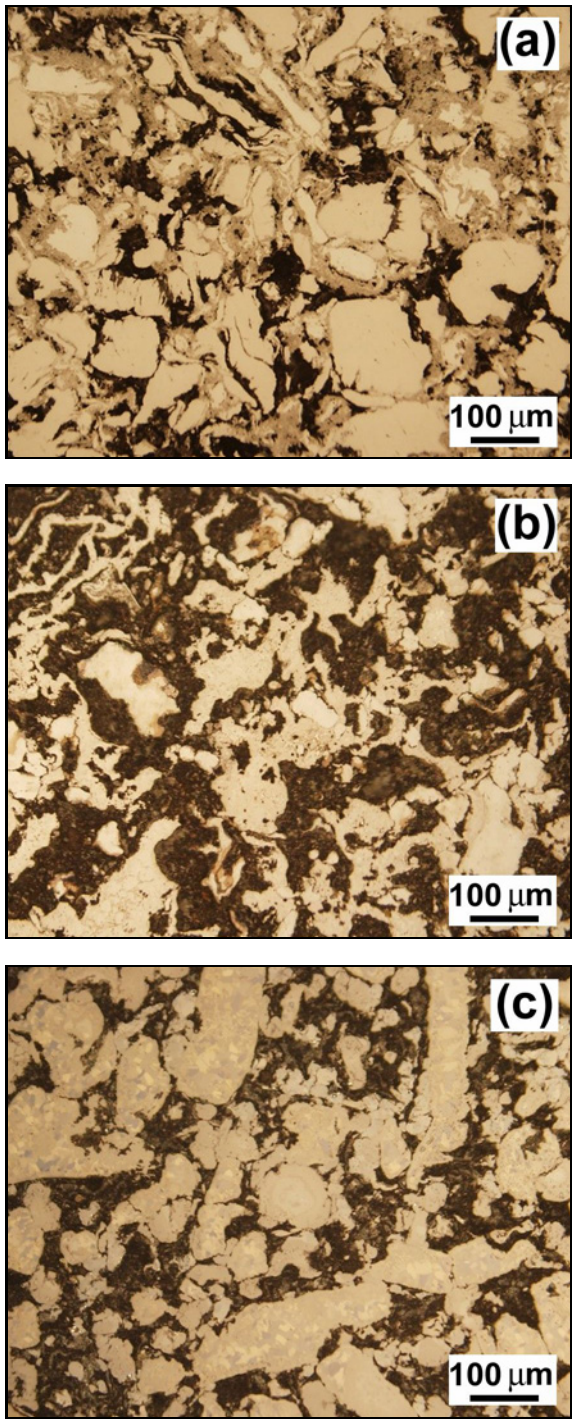

Fig. 5. Light-optical microstructures of individual studied composites: (a) composite A1, (b) composite A2, and (c) composite A3.

tives, which may be due to the enhanced reinforcing kinetics thanks to graphene nanoplatelets dispersion mechanisms. The results of XRD phase analyses of individual composites are shown in Fig. 6.

3.2. Tribological behavior

3.2.1. Coefficient of friction

The dynamic friction coefficients (COF) of A1–A3 with respect to time are shown in Fig. 7 at sliding speeds from 100 to 300 mm s^{-1} under 3 N.

When sliding a 100Cr6 steel ball against composite A1, the COF at all sliding speeds is about 0.4 at first approx. 500 s, then oscillates between 0.3 and 0.5. But at the sliding speed of 100 mm s^{-1}, the COF

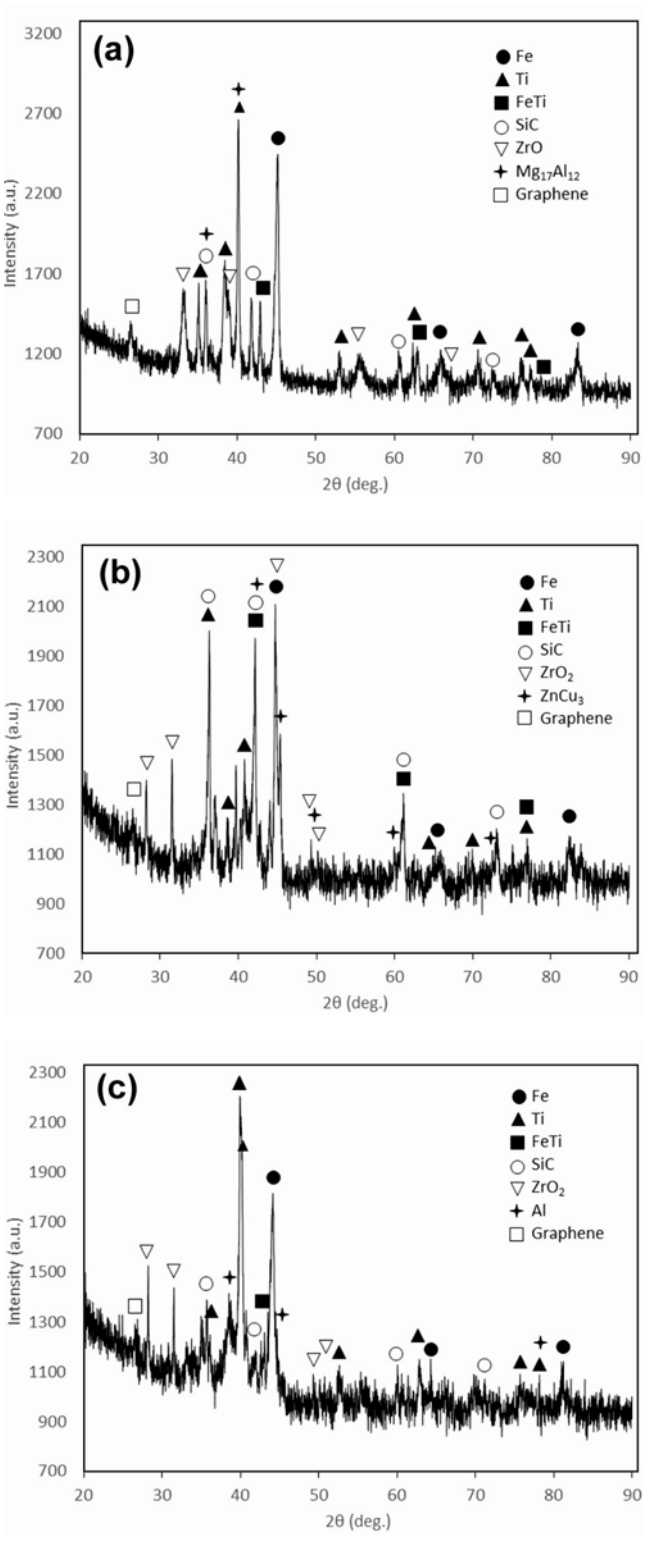

Fig. 6. XRD phase analyses of individual composites: (a) composite A1, (b) composite A2, and (c) composite A3.

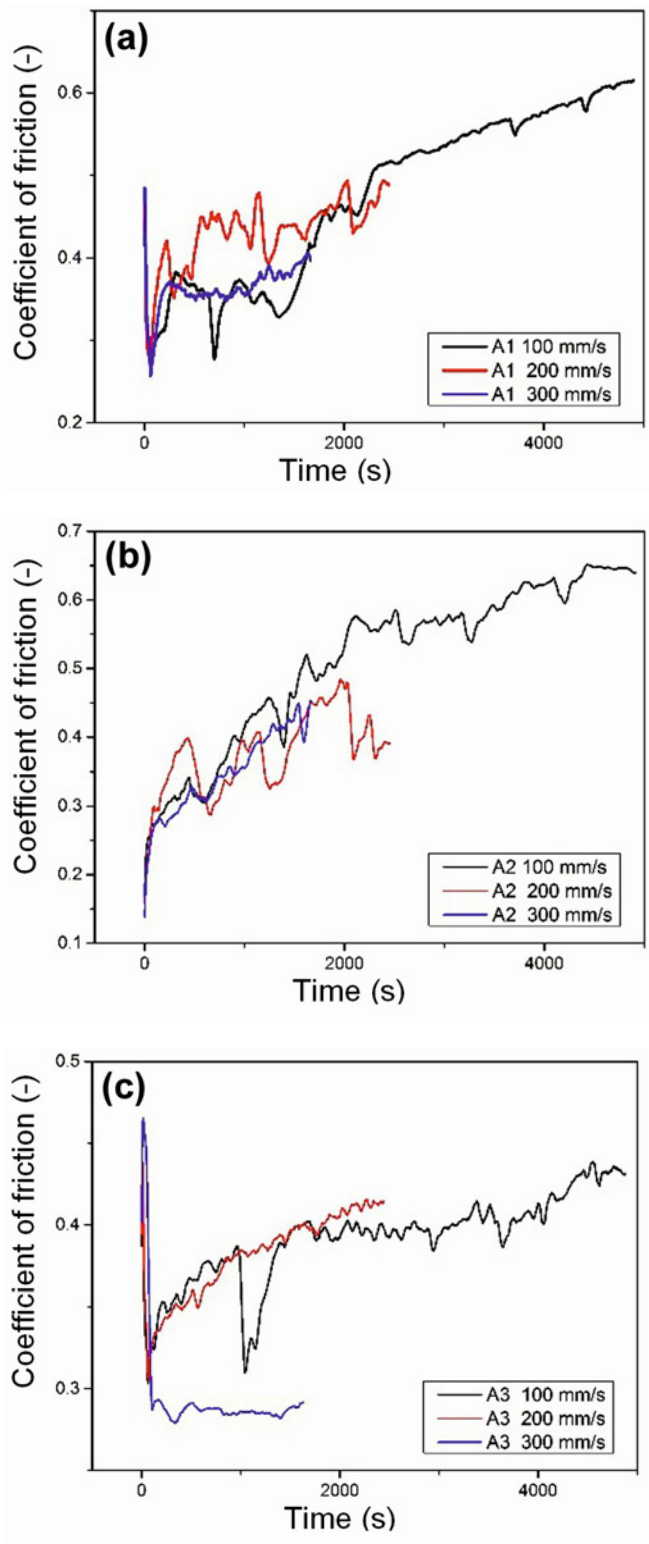

Fig. 7. Coefficient of friction vs time: (a) composite A1, (b) composite A2, and (c) composite A3.

slightly increased to 0.6. It was caused thanks to adhesive/abrasive mechanisms at the dry sliding without lubricant. In general, COF can be divided into two stages: the first stage – trial run and the second stage – stable running. At the speed of 100 mm s^{-1} and with increasing sliding time, the COF increased for A1, A2,

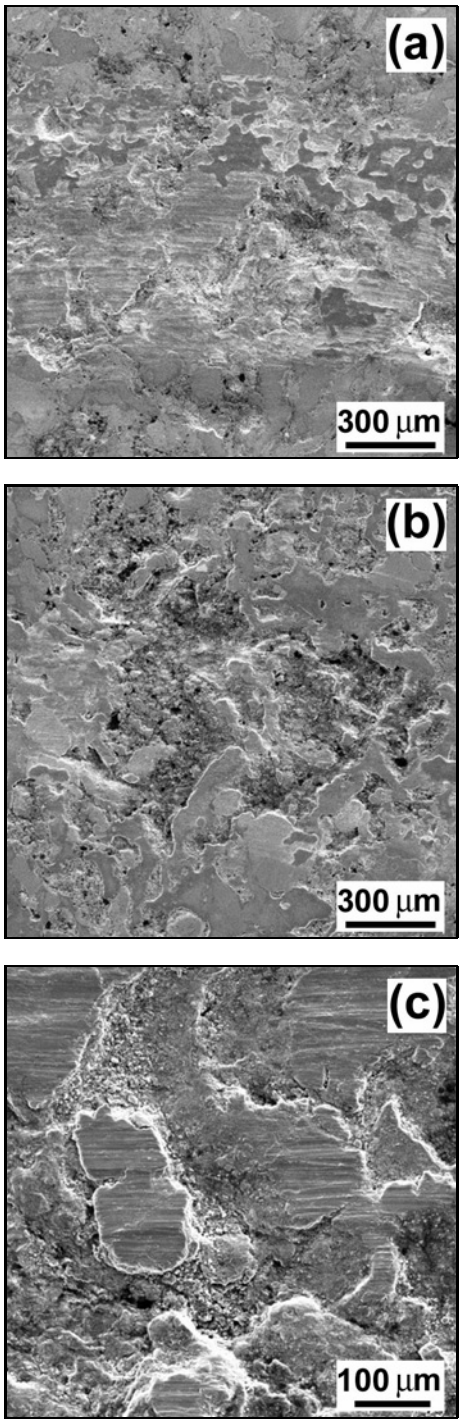

Fig. 8. SEM images of tribo-tracks: (a) composite A1, (b) composite A2, and (c) composite A3.

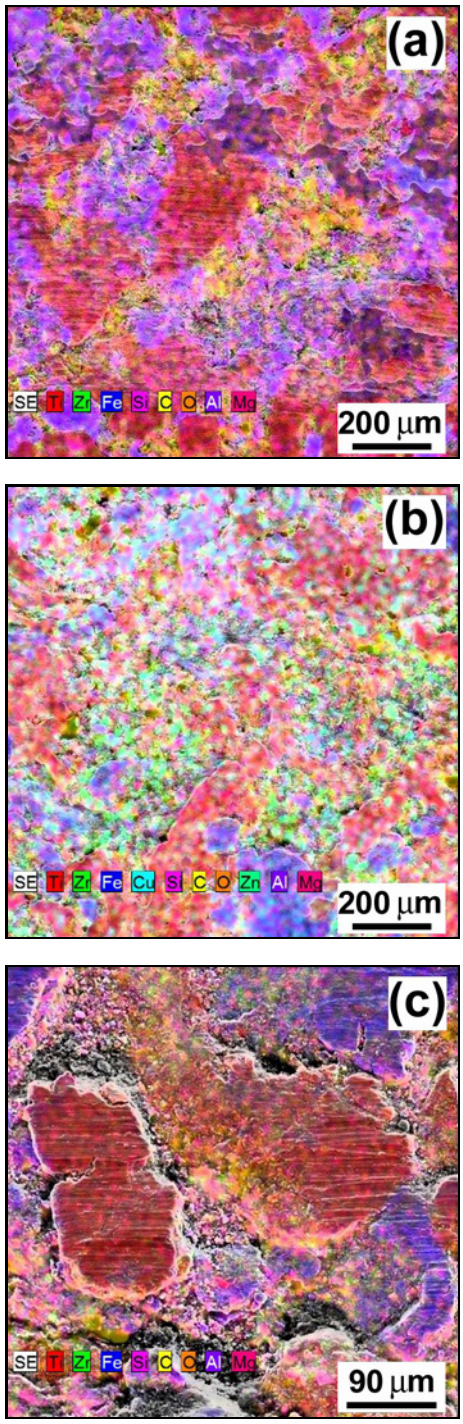

Fig. 9. EDXS maps of worn surfaces: (a) composite A1, (b) composite A2, and (c) composite A3.

and A3 composites up to 0.65. As the sliding speed increases up to 300 mm s^{-1}, the real contact area and asperities meshing of the friction pairs increase. Thus, there is an apparent decrease in the friction coefficient down to approx. 0.4. This is because the higher sliding speed results in faster surface rubbing and a higher surface temperature. Then, the high temperature may lead to the softening of the surface, meanwhile improving the deformation ability, so the surface roughness and friction coefficient are both decreasing [5, 9].

3.2.2. Wear behavior

Figure 8 shows the SEM micrographs of the worn surfaces of A1–A3 samples sliding against 100Cr6

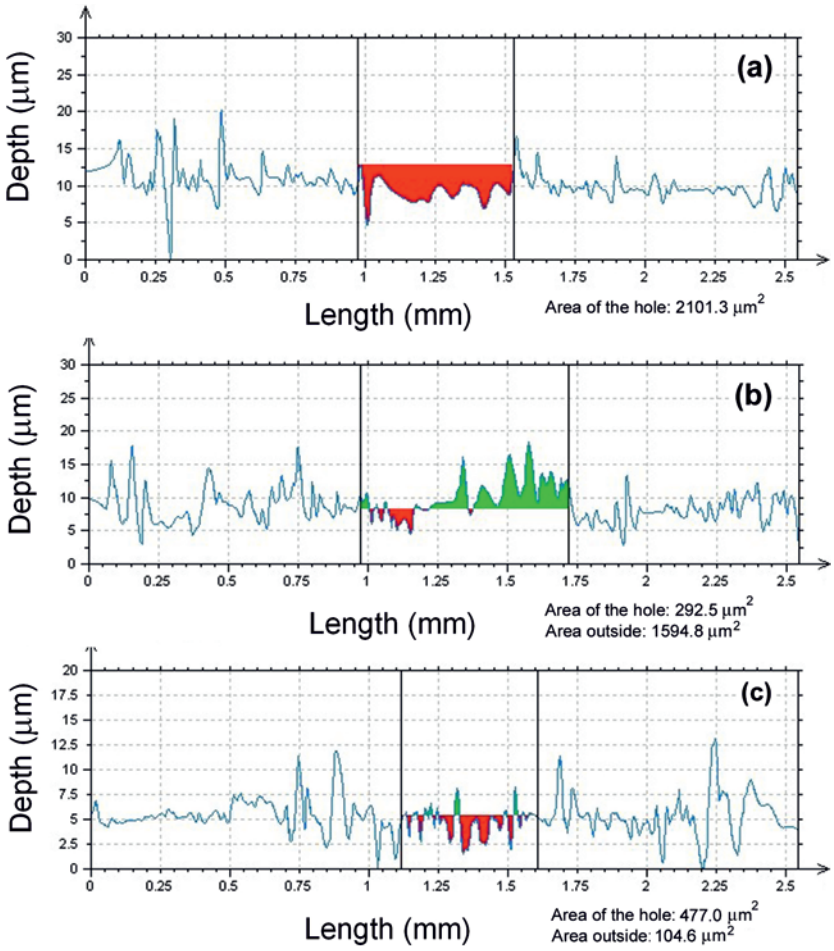

Fig. 10. Tribo-track profiles of sample A1 after tribological tests at various sliding speeds: (a) 100 mm s^{-1}, (b) 200 mm s^{-1}, and (c) 300 mm s^{-1}.

bearing steel ball at 3 N and 100–300 mm s^{-1}.

Discontinuous layers are observed on the worn surfaces of A1 and A3 samples. EDXS maps of worn surfaces are presented in Fig. 9.

SEM images of worn samples revealed that matrix breakage and ploughing reduced as the sliding speed increased. This shows that adding Al and, to a lesser extent, MgAl significantly impacts the wear properties of A3 and A1 composites. The higher surface temperature at the higher speed of 300 mm s^{-1} (in the case of sample A3) favors the formation of wear debris and its adverse effects on the increased wear. In the case of A1 and A2 composite, wear is significantly lower, probably because there are small changes in the surface performance of the materials, and it is influenced by the mechanical roughness degree, the molecular attraction of the surface and interfacial strength, respectively. In Fig. 10, the tribo-track profiles of sample A1 are shown for various sliding speeds. During the tribological test, sample A3, with the addition of Al, had major material exfoliation in the area of the tribo-track after the tribo test at 300 mm s^{-1} (see Fig. 11). This disruption of the material during the tribological

Fig. 11. Tribo-tracks of composites A1, A2, A3 (from left to right) after completed tribological tests at sliding speeds 100, 200, and 300 mm s^{-1}.

test is also documented on the COF vs time graph, Fig. 7. The wear resistance for individual experimental composites and used sliding speeds was determined by measuring the average weight loss. The obtained results are summarized in Table 4.

In Fig. 12, flat patches were observed, and a slight decrease in the depth and width of the track profile at the corresponding axonometric plot of the A1 composite.

The appearance of smooth stripes illustrates the

Table 4. Weight loss values of studied composites for applied tribological test conditions (applied load 3 N, sliding distance 500 m, sliding speed from 100 to 300 mm s^{-1})

Composite	Sliding speed (mm s^{-1})	Average weight loss (g)
A1	100	0.0035
	200	0.0051
	300	0.0163
A2	100	0.0369
	200	0.0124
	300	0.0187
A3	100	0.3245
	200	0.0225
	300	0.1080

plastic deformation of the sample surface created in the sliding at the slowest speed (Fig. 10a). At higher sliding speed, the cracks caused by the fatigue effect are propagated to the surface, thus resulting in the micro-scale fragmentation and exfoliation of materials (Fig. 10b). However, at the highest sliding speed, the wear of A1 composite is more moderate (Fig. 10c). These typical properties represent the typical abrasive wear behavior [19]. In Fig. 11, it is seen for A1 and A2 composites that there are no deep furrows on the worn surfaces, and the edge of the wear scar is smooth and flat, indicating that the wear resistance of A1 and A2 composites is significantly better in the comparison to the A3 composite. Current experiments were carried out at room temperature; therefore, in our future work, it will be desirable to perform tribological tests on the examined composites at elevated temperatures and higher loads to assess the suitability of their application under high temperature (up to 300 °C) friction conditions.

4. Conclusions

This work dealt with the friction properties of metal-ceramic composites enriched by waste metal powders and chips, namely the preparation and characterization of Ti-Fe-MgAl (CuZn, Al) metals, ZrO_2-SiC ceramics and incorporated graphene nanoplatelets (GNPs). In the experimental part of this work, examined composite samples were prepared from recycled and commercial powder components by spark plasma sintering (SPS) at a temperature of 1000 °C and 50 MPa sintering pressure to prepare composites with near to 100 % density (non-porous). We investigated the suitability of using waste metallic materials as an additive or enrichment of the metal-ceramic matrix of materials for friction applications. We studied

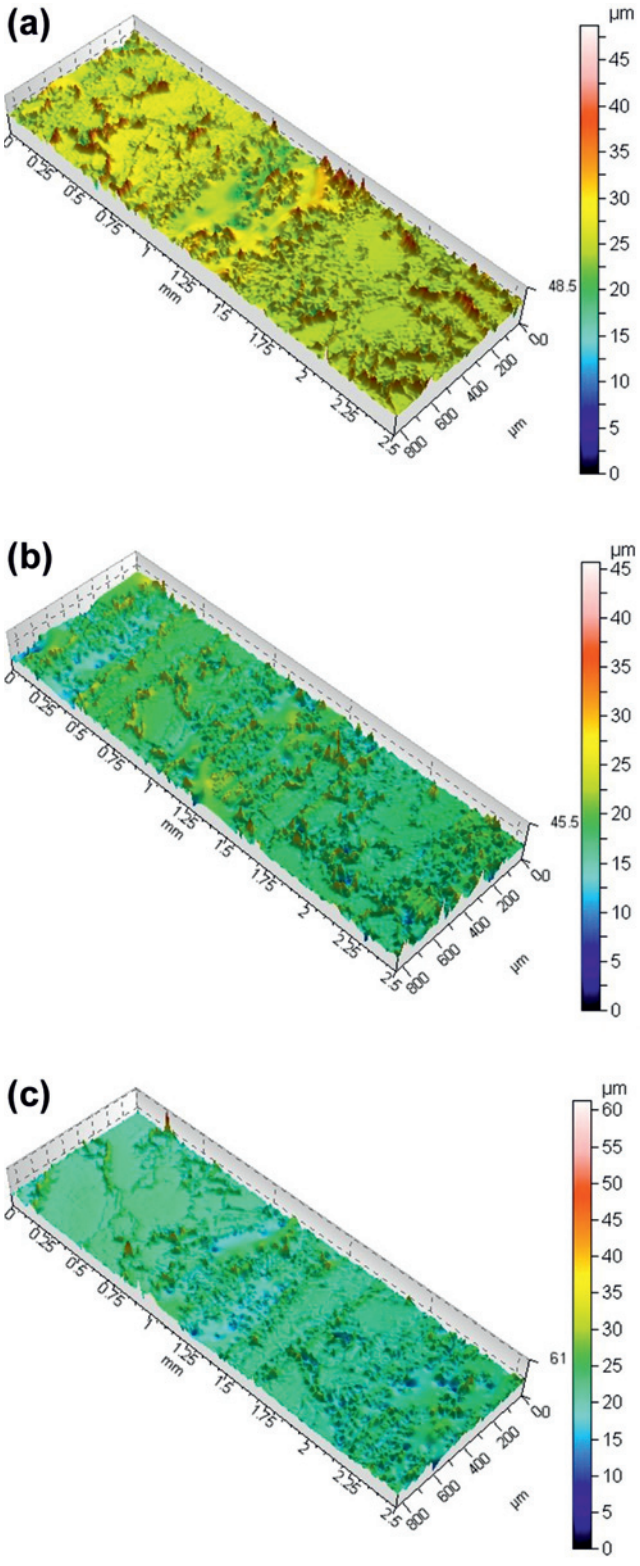

Fig. 12. Axonometric plots of wear tracks on A1 composite obtained from wear tests under dry sliding conditions at various sliding speeds: (a) 100 mm s^{-1}, (b) 200 mm s^{-1}, and (c) 300 mm s^{-1}.

the effect of adding these waste materials concerning their effect on sintering and, subsequently, on the tribological properties of the composites. The obtained results are summarized in the conclusions below:

1. The basis of the matrix of the studied composites was Ti and Fe in the ratio of 40 wt.% and 25 wt.%, taking into account the results of previous experiments [17], where it was shown that this ratio had the most favorable effect on both COF and wear values.

2. The sintering parameters (1000 °C, 50 MPa, 10 min) of the studied composites, to ensure the highest possible compaction, seem to be sufficient concerning the achieved values of COF, hardness and wear resistance for the composite with the addition of MgAl (A1 sample) showing slight abrasive wear behavior with probable micromachining or low-cycle fatigue wear mechanism.

3. Tribological tests performed at speeds 100, 200, and 300 mm s^{-1} show that the COF values varied with speed, peaking at about 0.65 at 100 mm s^{-1} and with increasing speed, there was an apparent reduction down to about 0.4, which may have been affected by faster surface rubbing and higher surface temperature which leads to softening the surface.

4. This study has shown that the SPS sintering technique can be used to fabricate Ti-Fe matrix waste metal friction composites. The obtained results on wear resistance indicated that the 40Ti-25Fe-15MgAl-10ZrO_2-5SiC-5GNPs metal-ceramic composite (sample A1) shows the most promising potential for demanding friction applications.

Acknowledgements

This work was supported by the projects VEGA 2/0101/20 and APVV-18-0438. The authors wish to thank Dr. F. Kromka (IMR SAS, Košice, Slovakia) for performing XRD phase analyses.

References

[1] V. B. Bhandari, Design of Machine Elements. Tata McGraw-Hill (2010). pp. 472. ISBN 9780070681798. Retrieved 9 February 2016.

[2] "Definition of brake". The Collins English Dictionary. Collins COBUILD Key Words for Automotive Engineering. Harper Collins Publishers (2016). https://www.collinsdictionary.com/dictionary/english/brake

[3] M. Kchaou, A. Sellami, J. Fajoui, R. Kus, R. Elleuch, F. Jacquemin, Tribological performance characterization of brake friction materials: What test? What coefficient of friction?, Proc. ImechE Part J: J. Engineering Tribology 233 (2019) 214–226. https://doi.org/10.1177/1350650118764167

[4] F. Findik, Latest progress on tribological properties of industrial materials, Mater. Des. 57 (2014) 218–244. https://doi.org/10.1016/j.matdes.2013.12.028

[5] K.W. Liew, U. Nirmal, Frictional performance evaluation of newly designed brake pad materials, Mater. Des. 48 (2013) 25–33. https://doi.org/10.1016/j.matdes.2012.07.055

[6] X. J. Shen, X. Q. Pei, Y. Liu, S. Y. Fu, Tribological performance of carbon nanotube-graphene oxide hybrid/epoxy composites, Compos. Part B-Eng 57 (2014) 120–125. https://doi.org/10.1016/j.compositesb.2013.09.050

[7] Y. Ma, Y. Liu, S. Ma, H. Wang, Z. Gao, J. Sun, J. Tong, L. Guo, Friction and wear properties of dumbbell-shaped jute fiber-reinforced friction materials, J. Appl. Polym. Sci. 131 (2014) 40748. https://doi.org/10.1002/app.40748

[8] Y. Liu, Y. Ma, X. Lv, J. Yu, J. Zhuang, J. Tong, Mineral fibre reinforced friction composites: Effect of rockwool fibre on mechanical and tribological behaviour, Mater. Res. Express 5 (2018) 095308. https://doi.org/10.1088/2053-1591/aad767

[9] https://www.bridgestonetire.com/learn/maintenance/ceramic-vs-metallic-brake-pads/#%CB%83, 1.4.2021, ©2022 Bridgestone Americas Tire Operations, LLC.

[10] R. K. Uyyuru, M. K. Surappa, S. Brusethaug, Tribological behavior of Al-Si-SiCp composites/automobile brake pad system under dry sliding conditions, Tribol. Int. 40 (2007) 365–373. https://doi.org/10.1016/j.triboint.2005.10.012

[11] T. Peng, Q. Yan, G. Li, X. Zhang, Z. Wen, J. Xuesong, The braking behaviors of Cu-based metallic brake pad for high-speed train under different initial braking speed, Tribol. Lett. 65 (2017) 135. https://doi.org/10.1007/s11249-017-0914-9

[12] K.W. Liew, U. Nirmal, Frictional performance evaluation of newly designed brake pad materials, Mater. Design 48 (2013) 25–33. https://doi.org/10.1016/j.matdes.2012.07.055

[13] P. Zhang, L. Zhang, K. Fu, J. Cao, C. Shijia, X. Qu, Effects of different forms of Fe powder additives on the simulated braking performance of Cu-based friction materials for high-speed railway trains, Wear 414–415 (2018) 317–326. https://doi.org/10.1016/j.wear.2018.09.006

[14] J. Bijwe, Multifunctionality of non-asbestos organic brake materials. In: Multifunctionality of polymer composites, challenges and new solutions, (2015) 551–572. https://doi.org/10.1016/B978-0-323-26434-1.00017-9

[15] C. Hong, G. Xun, H. Yun-Feng, Automotive control: The state of the art and perspective, Acta Autom. Sin. 39 (2013) 322–346. https://doi.org/10.1016/S1874-1029(13)60033-6

[16] J. Song, Performance evaluation of a hybrid electric brake system with a sliding mode controller, Mechatronics 15 (2005) 339–358. https://doi.org/10.1016/j.mechatronics.2004.09.005

[17] M. Podobová, V. Puchý, L. Falat, R. Džunda, M. Besterci, P. Hvizdoš, Microstructure and tribological behavior of SPS processed Fe/Ti-15wt.%Cu-based metal matrix composites with incorporated waste Ti-chips, Kovove Mater. 58 (2020) 83–91. https://doi.org/10.4149/km_2020_2_83

[18] F. Makni, M. Kchaou, R. Elleuch, A.-L. Cristol, Y. Desplanques, Impact of the Mixing of Ingredients on the Heterogeneity of Organic Brake Lining Materials.

In: Europe's Braking Technology Conference & Exhibition EURO BRAKE 2015, Dresden, Germany, 4–6 May 2015.

[19] Y.-S. Lee, Y. Kondo, M. Okayasu, Friction-induced martensitic transformation and wear properties of stainless steel under dry and wet conditions, Metals 10 (2020) 743. https://doi.org/10.3390/met10060743